EXPERIMENTAL STUDIES ON MICRO-VORTEX GENERATORS IN HYPERSONIC FLOW

M.R. Saad*, A. Che Idris* and K. Kontis**
*Faculty of Engineering, Universiti Pertahanan Nasional Malaysia,
Kuala Lumpur 57000 Malaysia
**School of Mechanical Aerospace & Civil Engineering, University of Manchester,
Manchester M13 9PL United Kingdom
k.kontis@manchester.ac.uk

Abstract

Shock/boundary layer interaction (SBLI) is an undesirable phenomenon occurring in high-speed propulsion systems. The conventional method to manipulate and control SBLI is using a bleed system that removes a certain amount of mass of the inlet flow to control boundary layer separation. However the system requires larger nacelles to compensate the mass loss and this contribute to additional weight and drag and reduce the overall performance. This study investigates a novel type of flow control device called micro-ramps, a part of the micro-vortex generator (VGs) family that intends to replace the bleed technique. Micro-ramps produce pairs of counter-rotating streamwise vortices, which help to suppress SBLI and reduce the chances of flow separation. Experiments were done at Mach 5 with 3 micro-ramp models of different sizes. High-speed schlieren photography, oil-dot visualization, surface flow visualization and infrared thermography were used in this investigation. The results revealed the detailed flow characteristics of the micro-ramp, such as the primary and secondary vortices. This helps us to understand the overall flow physics of micro-ramps in hypersonic flow and their application for SBLI control.

1 Introduction

The prominent problem faced by the air-breathing propulsion system of hypersonic aero-vehicles is the phenomenon known as shock wave- boundary layer interactions (SBLI) which cause boundary layer separation and adverse pressure gradients. This eventually lead to total pressure loss and flow distortion in the intake section of the engine [1,2]. These reduce the overall propulsive efficiency of a hypersonic vehicle. Therefore it is essential to apply flow control mechanisms either at the beginning or throughout the interaction itself to prevent the boundary layer from separating and at the same time to maintain a high rate of efficiency even at off design conditions.

Micro-ramp is a recently developed novel flow control device that has shown potentials in solving the adverse phenomena [3-6]. It is a part of the micro-vortex generator family. The term 'micro' refers to the device having the height smaller than the thickness of the boundary layer, δ. Most of the literatures at present stated the percentage of the micro-ramp height to δ of the flow is between 30% and 90% [5, 7-10]. The small size of the micro-ramp allows it to be embedded inside the boundary layer hence reducing the parasitic drag relative to the conventional full size vortex generator. The other advantages of utilizing this passive-type flow control device are cost-effective, physically robust and independent of power source.

The initial idea on using micro-ramp in controlling SBLI was introduced by Babinsky *et al.* [11]. The geometries of the micro-ramp proposed by Anderson *et al.* [7] were used in their experimental investigation at Mach 2.5. From their results it was found that the counter-rotating streamwise vortices generated by the

micro-ramp helped to suppress the SBLI effect. The upwash and downwash motion produced by the vortices improved the state of the boundary layer by simultaneously bringing the high-momentum flow from the outer regions towards the wall surface. Hence a healthier and more robust boundary layer that is less prone to separation is produced.

Numerical investigation done by Li & Liu [9,10] detailed the flow characteristics in the micro-ramp downstream region. They found a chain of vortex rings structure originating from the apex of the micro-ramp due to Kelvin-Helmhotz instability [12,13]. These ring structures travel further downstream and interact with the impinging shock wave eventually distorting the structure of the shock wave hence reducing its strength [15]. The experiments of Lu *et al.* [16,17] and Sun *et al.* [18] corroborated the numerical findings of Li & Liu [9,10] and identified the existence of the vortex rings.

The majority of the previous studies on micro-ramps mentioned previously were done in supersonic conditions therefore it is essential to perform investigations on the capability of micro-ramps in manipulating hypersonic flow and consequently improve the boundary layer caused by SBLI. The main objective of this study is to provide qualitative analysis of the flow behavior over and downstream the micro-ramp at Mach 5 by revealing the main flow features using high-speed schlieren photography, oil-dot visualization, surface flow visualization and infrared thermography.

2 Experimental Setup & Flow Diagnostics

2.1 High Supersonic Tunnel (HSST)

The experiments are conducted at Mach 5 in the HSST, a hypersonic blow-down wind tunnel with a unit Reynolds number of 13.2×10^6 m^{-1}. The stagnation pressure of the wind tunnel was set at 6.50×10^5 Pa ($\pm 5 \times 10^3$ Pa) and stagnation temperature of 375 K (± 5 K). The freestream Reynolds number fluctuates no more than 3.7%.

2.2 Micro-Ramps

For this investigation, 3 micro-ramp models named MR80, MR60 and MR40 were tested. The micro-ramps were manufactured in array configuration on top of a metal strip as shown in Figure 1. Table 1 lists the detail dimensions of the models for comparison with reference to the micro-ramp diagram shown in Figure 2.

Fig. 1. Micro-ramp models of MR40 (left), MR60 (middle) and MR80 (right).
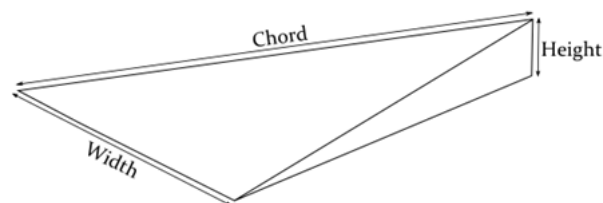
Fig. 2. Diagram of micro-ramp dimensions.

Dimensions (mm)	MR80	MR60	MR40
Height, h	4.64	3.48	2.32
Chord, c	33.4	25.1	16.7
Width, w	27.2	20.4	13.6

Table 1. Micro-ramp dimensions for comparison.

MR80, MR60 and MR40 have heights of 80%, 60% and 40% respectively of δ where δ is defined as the distance from the wall to a point where the velocity of the flow has reached the freestream velocity, U_∞. The dimensions listed in Table 1 were based on the design by Anderson *et al.* [7]. The ratio of dimensions are given as $s/h = 7.5$ and $c/h = 7.2$. The models were fixed to a 360mm long, 60 mm wide and 5 mm thick aluminium alloy flat plate.

2.3 Schlieren Photography

The Aero-Physics Laboratory of the University of Manchester us equipped with a Toepler's z-type schlieren system which consists of a Palflash 501 (Pulse Photonics) continuous light source together with a focusing lens and a 2 mm wide slit, two f=9 parabolic silver coated mirrors, a knife-edge and a Hoya 49 mm + 2 macro lens for focusing purposes. A Canon digital SLR camera EOS-450D 12MP is used to capture still images while a Photron APX-RS high-speed video camera is also employed for high-speed image recording at 10,000 fps.

2.4 Oil-dot Visualization

Oil-dot visualization is a technique that is used to visualize the flow pattern on the surface of a body. It is a representation of the behavior at the near wall flow. Discrete dots were applied on the surface of the model and their final condition will reveal the flow condition such as flow separation, laminar, transition and turbulent. The dots were made from the combination of linseed oil, silicon oil and titanium dioxide (TiO$_2$) powder. 0.5 mm blobs were then applied onto the plate using a syringe.

2.5 Surface Flow Visualization

The oil-flow recipe used in the current setup consists of paraffin, fluorescent colour powders, silicon oil and oleic acid. The fluorescent powder used has an average grain size of 10 µm. Two UV light sources with 20 W fluorescent tubes were mounted at a 45° angle on both sides of the test section windows to illuminate the model.

A Digital SLR camera, Nikon D90 12.3 million pixels with 18-105 VR lens was used to record high-definition videos of the run at 24fps and 1,280 × 720 resolution. VirtualDub, an open source software were then used to extract individual images.

The flat plate and the micro-ramps were both painted matt-black to increase the contrast between the fluorescent oil and the flat plate. An area of 60 mm × 60 mm was drawn 30 mm upstream from the micro-ramp leading edge to mark the location where the paint would be deposited. A 5 mL syringe was then used to apply the paint onto the model so that the paint did not spill and flow outside the dedicated boundary.

2.6 Infrared Thermography

The infrared (IR) camera used for this investigation was a FLIR Thermacam SC 3000 Cooled System. It is capable of measuring temperature ranging from -250K to 1,730 K with an accuracy of ±2% or ±2K. It is equipped with GaAs QWIP detector with resolution of 320 × 240 pixels and cooled to 70K in less than 6 minutes. The recording frequency of the camera is 50 Hz. The camera has to be kept at ambient pressure and therefore mounted on top of the test section at an angle of 15° from the vertical plane. The window on the top of the test section is specially made from Germanium (Ge) which is a commonly used material for infrared thermography. It has a high index of refraction and good IR transmission. The camera is connected to a dedicated PC to record and store the images.

2.7 Shock-Generator Setup

In order to investigate the effectiveness of micro-ramps in controlling SBLI, an oblique shock wave needs to be generated and eventually impinge on the flat plate downstream the micro-ramp. A shock-generator is installed by mounting it to the ceiling of the test section. The shock-generator creates a 34° oblique shock and impinges at 14.2δ downstream the center of the micro-ramp. However the result of the experiments with the presence of this shock-generator will only be reported in the schlieren photography section.

3 Results

Figure 3 shows the instantaneous schlieren images for all the models. A strong shock wave can be easily observed originating from the micro-ramp leading edge and a weaker shock wave can be seen at the trailing edge of the

model. The other shock waves that are also visible are the nozzle cone shock and the flat plate leading edge. The sudden growth of boundary layer was observed as it approaches the micro-ramp. It can also be seen that the micro-ramp is fully submerged inside the boundary layer hence satisfying the criterion of a micro vortex-generator explained earlier in Section 1.
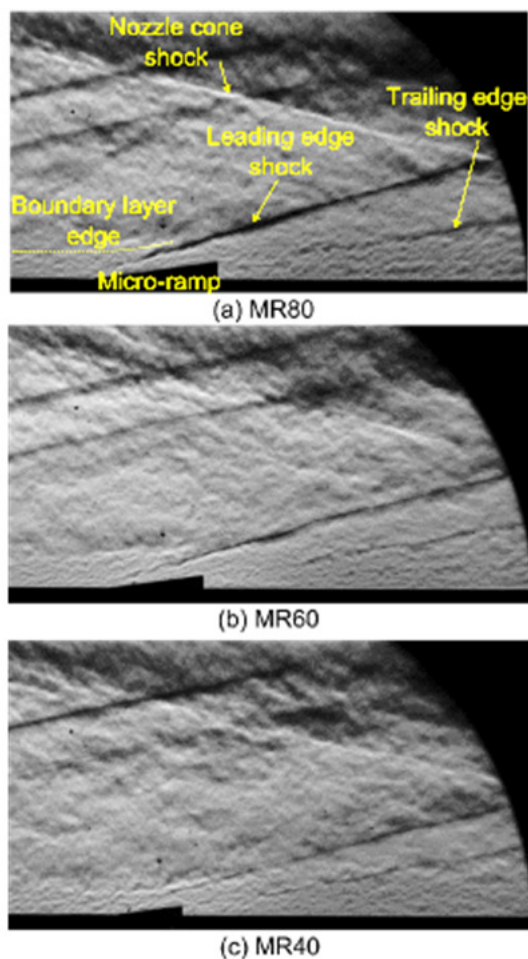
Fig. 3. Instantaneous high-speed schlieren images of micro-ramps without incident shock captured at 10,000 fps.

The shock structures of all three models are similar. However a thicker shock line originating from the leading edge of MR80 is clearly observable in Figure 3(a) compared to the other two models in Figure 3(b,c). This is the indication of a stronger shock wave due to the size of the model. The same case is observed in the case of the trailing edge shock where

MR80 produced a slightly stronger and more visible shock wave.
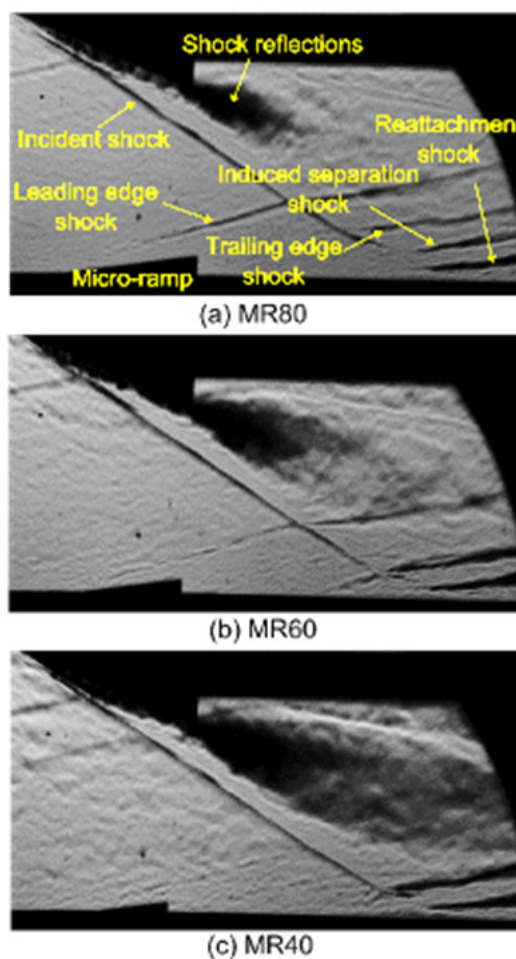
Fig. 4. Instantaneous high-speed schlieren images of micro-ramps with incident shock captured at 10,000 fps.

The existence of both the induced separation shock wave and reattachment shock wave in Figure 4 is a clear evidence of the occurence of SBLI in the case where the incident shock is presence. The incident shock wave impinging on the flat plate caused the hypersonic boundary layer to separate consequently producing the induced separation shock upstream the separation region and the reattachment shock further downstream. The shock reflections visible is caused by the flat plate leading edge shock impinging on the shock-generator and eventually being reflected away. Assessing qualitatively the effect of micro-ramps in controlling SBLI, the schlieren images in Figure 4 shows that the separation

and reattachment shock in Figure 4(a) are thinner compared to Figure 4(b,c). This means that MR80 managed to reduce the size of the boundary layer separation significantly hence producing lower intensity shock waves.
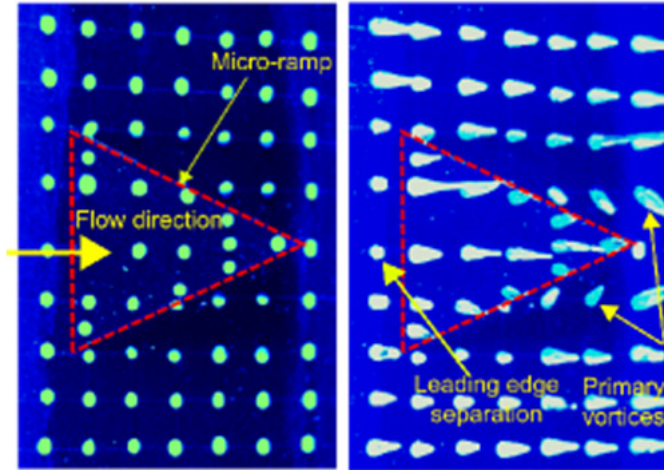
Fig. 5. Oil-dot visualization before (left) and after (right).

The condition of the oil-dots before and after the test are shown in Figure 5. It can be observed that the oil dots moved during the run and due to the high temperature flow, the oil dots dried leaving white streaks on the model surface. Focusing at the top of the micro-ramp surface, the flow at the centreline travels downstream in a straight line towards the trailing edge apex. The flow on both sides of the centreline tendsto curve to the slant edges of the micro-ramp.

A small separation region exists at the leading edge of the micro-ramp, indicated by the undisturbed oil-dots. Theoretically separation regions have lower skin friction coefficient therefore the oil-dots were less affected by the incoming flow. The separation region was induced by the small leading edge angle measured to be 8.6° from the horizontal plane. This angle also created a shock wave that was observed earlier in the schlieren images in Figure 3 and 4.

The oil streaks at the rear of the micro-ramp proved the existence of the primary vortices. The direction of the primary vortices rotation downstream the micro-ramp can also be deduced by looking at the orientation of the oil

streaks. The oil-dots were swept by the vortices towards the centreline.
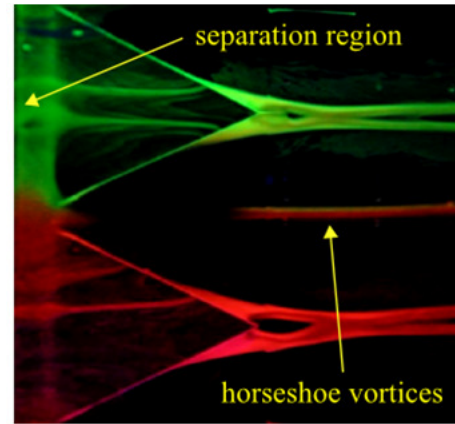
(a) MR80
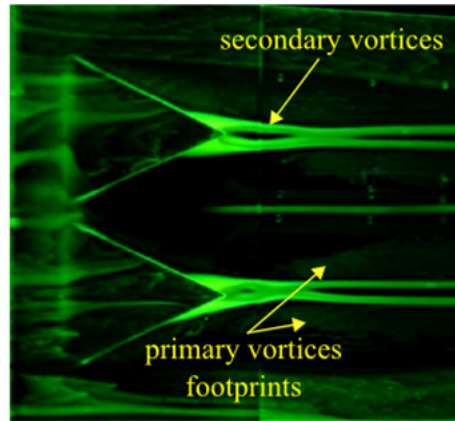
(b) MR60
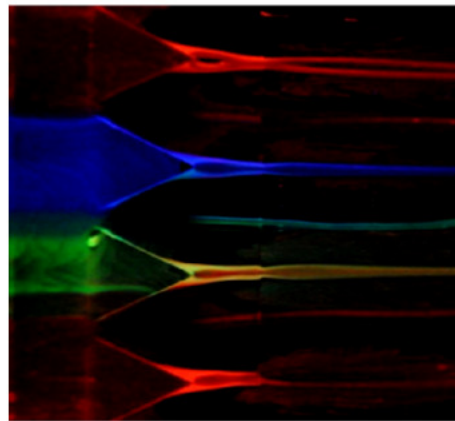
(c) MR40

Fig. 6. Surface flow visualization of micro-ramp in array configurations.

From the surface flow results shown in Figure 6, the leading edge separation ahead of the micro-ramp is clearly indicated by the oil acummulation. The flow on top of the micro-ramp moves towards the slant edges of both sides. The flow moving down the slant edges in

a rotational manner eventually transform into large vortices named primary vortices. The footprints of the primary vortices are visible in Figure 6(b). Another pair of smaller vortices can be observed wrapping around the micro-ramp shown by the oil thin oil streak known as the horseshoe vortices. The thick band of oil downstream the micro-ramp starts to divide into half creating another pair of vortices known as secondary vortices.
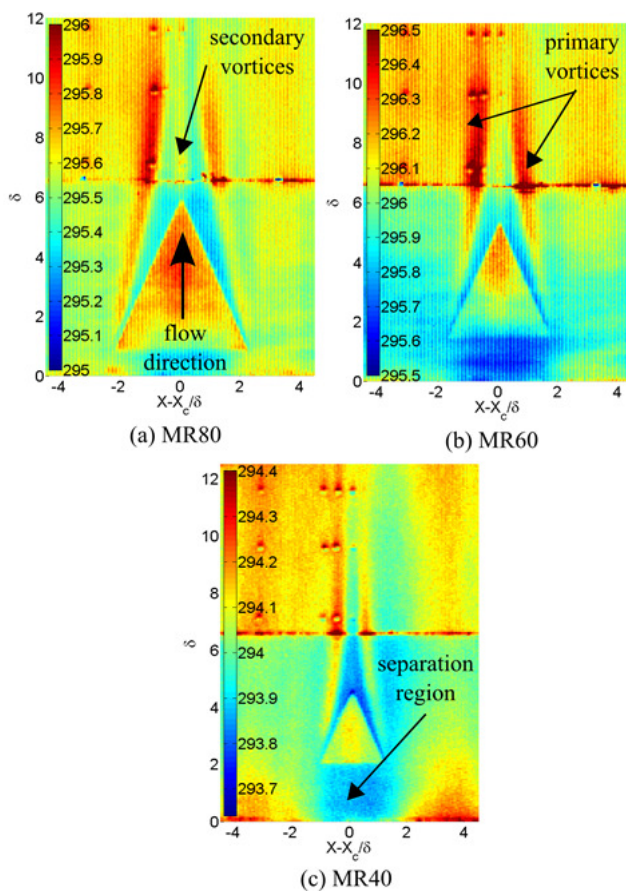
Fig. 7. Time-averaged infra-red images mapping the surface temperature.

The infra-red images in Figure 7 show the different sizes of the temperature streaks representing different sizes of the primary vortices for each models. The larger the micro-ramp the larger the primary vortices it produces. The primary vortices orginate at a location 0.5δ from the mciro-ramp leading edge. The separation regions are also visibile in the images indicated by the low temperature region in front of the micro-ramp leading edge. Due to

boundary layer separation, the flow was not able to transfer the heat to the near wall location hence a relatively colder area was formed.

The secondary vortices observed in the surface flow experiments in Figure 6 can also be seen in Figure 7(a,b) for MR80 and MR60 only. They suddenly exist in between the position of the primary vortices and propagate downstream. They are identified by slightly higher temperature streaks that start at a location 0.4δ downstream the apex of the model. However they are not visible in Figure 7(c) due to a weaker and smaller vortices being produced hence were not able to be captured by the IR camera.

4 Conclusions

The flow features of the micro-ramps have been characterized qualitatively using different experimental techniques. The high-speed schlieren exposed the basic shock structures of the micro-ramp and also the effect of the different sizes of micro-ramps in controlling SBLI. The largest micro-ramp, MR80 managed to reduce the SBLI effect better than the other models. The oil-dot visualization experiments revealed the leading edge separation region and also the direction of the primary vortices at the rear of the micro-ramp. The detail vortex structures downstream the micro-ramp were shown to be present in the surface flow visualization. The infra-red images revealed the point of origin of the vortices and also the existence of the separation region. Overall this study has contributed to the understanding of the basic flow physics involving micro-ramps and their role in controlling SBLI.

References

[1] Delery, J.M. Shock/Wave/Turbulent Boundary layer Interaction and its Control. *Progr. Aerosp. Sci.* **1985**, 209-280.

[2] Dolling, D.S. Fifty Years of Shock-Wave/Boundary-Layer Interaction Research: What Next? *AIAA Journal* **2001**, *39*, 1517-1532.

[3] McCormick, D.C. Shock/Boundary Layer Interaction Control with Vortex Generators and Passive Cavity. *AIAA Journal* **1993**, *31*, 91-96.

[4] Holden, H.; Babinsky, H. Effect of Microvortex Generators on Separated Normal Shock/Boundary Layer Interactions. *Journal of Aircraft* **2007**, *44*, 170-174.

[5] Lin, J.C. Review of Research on Low-Profile Vortex Generators to Control Boundary Layer Separation. *Progr. Aerosp. Sci.* **2002**, *38*, 389-420.

[6] Ashill, P.R.; Fulker, J.L.; Hackett, K.C. Research at DERA on Sub-Boundary Layer Vortex Generators (SBVG). AIAA Paper 2001-0887, 2001.

[7] Anderson, B.H.; Tinapple, J.; Surber, L. Optimal Control of Shock Wave Turbulent Boundary Layer Interactions Using Micro-Array Actuation. AIAA Paper 2006-3197, 2006.

[8] Blinde, P.L.; Humble, R.A.; van Oudheusden, B.W; Scarano, F. Effects of Micro-Ramps on a Shock Wave/ Turbulent Boundary Layer Interaction. *Shock Waves* **2009**, *19*, 507-520.

[9] Li, Q.; Liu, C. LES for Supersonic Ramp Control Flow using MVG at *M=2.5* and *Re$_\theta$=1440*. AIAA Paper 2010-0592, 2010.

[10] Li, Q.; Liu, C. Numerical Investigations on the Effects of the Declining Angle of the Trailing-Edge of MVG. AIAA Paper 2010-4623, 2010.

[11] Babinsky, H.; Li, Y.; Pitt Ford, C.W. Microramp Control of Supersonic Oblique Shock-Wave/Boundary-Layer Interactions. *AIAA Journal* **2009**, *47*, 668-675.

[12] Wang, K.C. Boundary Layer over a Blunt Body at High Incidence with an Open-Type of Separation. *Proc. R. Soc. Lond. A* **1974**, *340*, 33-35.

[13] Yan, Y.; Chen. C.; Wang, X.; Liu, C. LES Study on the Mechanism of Vortex Rings behind Supersonic MVG with Turbulent Inflow. AIAA Paper 2012-1093, 2012.

[14] Lu, P.; Yan, Y.; Liu, C. Numerical Study on Mechanism of Multiple Rings Formation. AIAA Paper 2012-0747, **2012.**

[15] Yan, Y.; Chen. C.; Wang, X.; Liu, C. LES Study on the Mechanism of Vortex Rings behind Supersonic MVG with Turbulent Inflow. AIAA Paper 2012-0047, **2012**.

[16] Lu, F.L.; Pierce, A.J.; Shih, Y.; Liu, C.; Li, Q. Experimental and Numerical Study of Flow Topology Past Micro Vortex Generators. AIAA Paper 2010-4463, **2010**.

[17] Lu, F.L.; Pierce, A.J.; Shih, Y. Experimental Study of Near Wake of Micro Vortex Generators in Supersonic Flow. AIAA Paper 2010-4623, 2010.

[18] Sun, Z.; Schrijer, F.F.K.; Scarano, F.; Oudheusden, B.W.V. PIV Investigation of the 3D Instantaneous Flow Organization behind a Micro-Ramp in a Supersonic Boundary Layer. In *Shock Waves*; Kontis, K., Ed.; Springer, Heidelberg, Germany, 2011.

Copyright Statement